Eur J Nucl Med Mol Imaging (2013) 40:1283–1291
DOI 10.1007/s00259-013-2408-9

REVIEW ARTICLE

Optical imaging as an expansion of nuclear medicine: Cerenkov-based luminescence vs fluorescence-based luminescence

Patrick T. K. Chin · Mick M. Welling · Stefan C. J. Meskers · Renato A. Valdes Olmos · Hans Tanke · Fijs W. B. van Leeuwen

Received: 18 January 2013 / Accepted: 21 March 2013 / Published online: 15 May 2013

Abstract Integration of optical imaging technologies can further strengthen the field of radioguided surgery. Rather than using two separate chemical entities to achieve this extension, hybrid imaging agents can be used that contain both radionuclear and optical properties. Two types of such hybrid imaging agents are available: (1) hybrid imaging agents generated by Cerenkov luminescence imaging (CLI) of β-emitters and (2) hybrid imaging agents that contain both a radioactive moiety and a fluorescent dye. One major challenge clinicians are now facing is to determine the potential value of these approaches. With this tutorial review we intend to clarify the differences between the two approaches and highlight the clinical potential of hybrid imaging during image-guided surgery applications.

Keywords Cerenkov · Fluorescence · Multimodal imaging · Image-guided surgery · Nuclear medicine

Electronic supplementary material The online version of this article (doi:10.1007/s00259-013-2408-9) contains supplementary material, which is available to authorized users.

P. T. K. Chin · M. M. Welling · R. A. Valdes Olmos · F. W. B. van Leeuwen (✉)
Interventional Molecular Imaging Laboratory, Department of Radiology, Leiden University Medical Center, P.O. Box 9600, 2300 RC Leiden, The Netherlands
e-mail: F.W.B.van_Leeuwen@lumc.nl

S. C. J. Meskers
Molecular Materials and Nanosystems, Eindhoven University of Technology, P.O. Box 513, 5600 MB Eindhoven, The Netherlands

R. A. Valdes Olmos
Department of Nuclear Medicine, Netherlands Cancer Institute-Antoni van Leeuwenhoek Hospital, Plesmanlaan 121, 1066 CX Amsterdam, The Netherlands

H. Tanke
Department of Molecular Cell Biology, Leiden University Medical Center, P.O. Box 9600, 2300 RC Leiden, The Netherlands

Introduction

Nuclear imaging modalities like gamma imaging [i.e. scintigraphy and single photon emission computed tomography (SPECT)] and positron emission tomography (PET) have proven valuable for molecular diagnostics and in surgical applications [1–3]. Their value is strengthened by the fact that these molecular imaging techniques can be complemented with detailed anatomical imaging using (integrated) computed tomography (CT) and/or magnetic resonance imaging (MRI) [4, 5]. The combination of different imaging signatures, united in a single imaging agent, allows for fully integrated multimodality imaging paradigms [6]. By complementing nuclear imaging agents with an optical read-out, it becomes possible to supplement radio-guidance technologies with optical identification during surgery (Fig. 1a) [7, 8], enabling true interventional molecular imaging.

The recent availability of sensitive, small and cost-effective digital imaging systems has enabled the introduction of real-time digital fluorescence imaging in surgical guidance applications. These imaging systems are mostly based on charge-coupled devices (CCD) and complementary metal–oxide–semiconductor (CMOS) imaging sensors with very low noise levels and high sensitivities [9–11]. Light emitting diodes (LEDs) and lasers are often used as dedicated

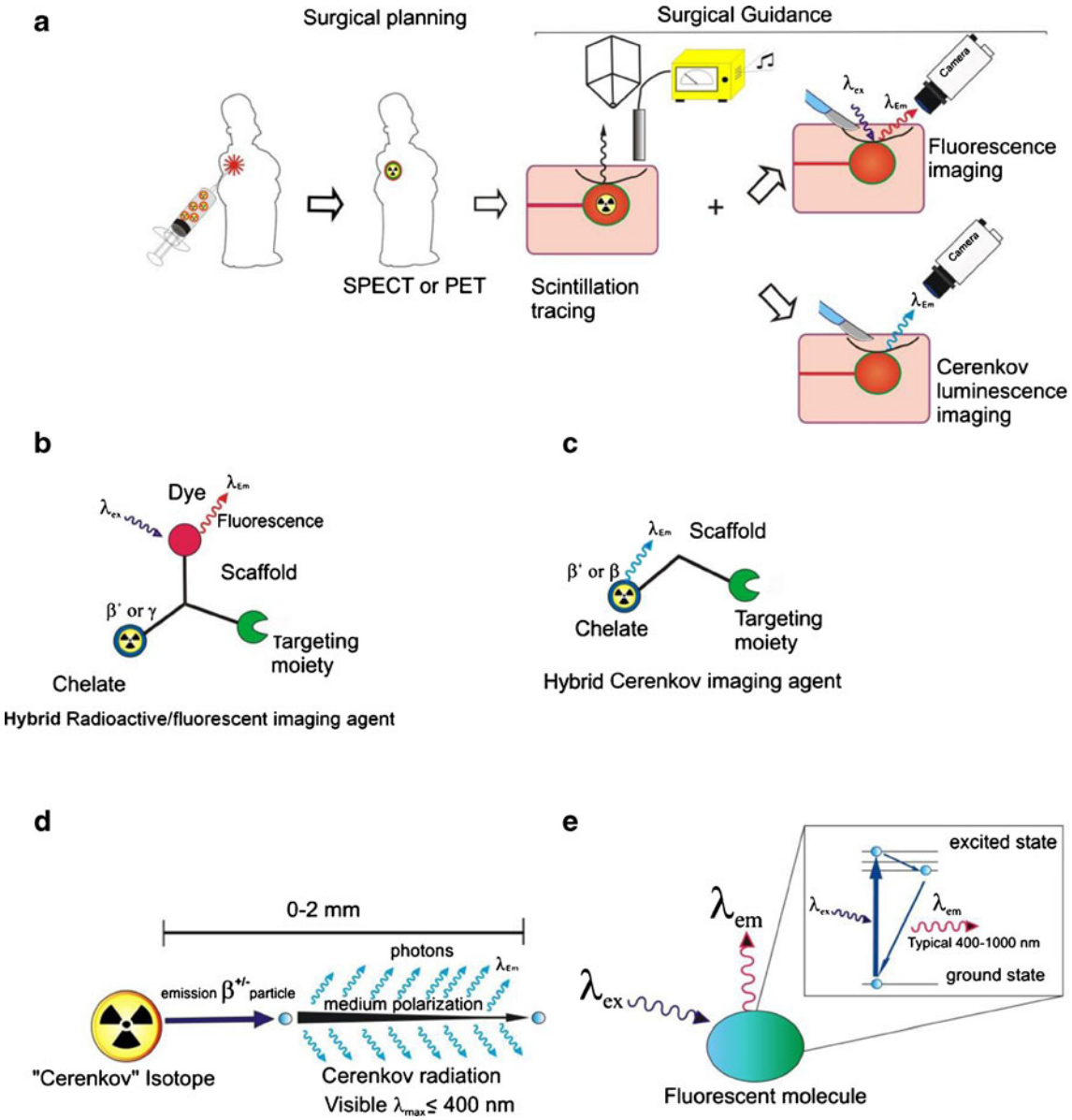

Fig. 1 Schematic representation of the value that hybrid imaging agents may provide during surgery. **a** Administration of a single (targeted) imaging agent that contains both a radioisotope and a fluorescent dye can be followed by preoperative visualization using the radioactive modality, followed by scintillation tracing and a real-time optical read-out during the surgical procedure. **b** A "conventional" hybrid imaging agent with a targeting modality for site selectivity, a radiolabel and a fluorophore. **c** A hybrid imaging agent involving a targeting moiety for site selection and a "Cerenkov" radiolabel. Schematic representation of the physical principles for the generation of light by **d** Cerenkov luminescence, showing the emission of a charged β particle, inducing the emission of Cerenkov photons along its pathway. **e** The principle of fluorescence, showing the excitation of a ground state electron followed by relaxation to the ground state under the emission of a photon

bright and relative narrow band excitation sources in these digital fluorescence systems [10, 12]. Alternative excitation light sources are often found in lasers and xenon lamps [10].

The inclusion of multiple signatures in single imaging agents is generally achieved via chemical modifications. For example, a hybrid imaging agent can be composed of a (targeted) molecular scaffold that is functionalized with both a radioactive and a fluorescent moiety (Fig. 1b). Alternatively, the detection of the Cerenkov luminescence (CL) emitted by β-emitters (both electrons and positrons, Fig. 1d) can potentially be used for optical detection [13]. This concept was first demonstrated, in a preclinical setting, by Robertson et al. in 2009 [14]. With the Cerenkov luminescence imaging (CLI) concept both a β-emission and a luminescence signature are integrated in a single "isotope". When applying CLI on clinically approved β-

emitters, e.g. PET tracers, one can regard these tracers as hybrid imaging agents (Fig. 1c). Validation and applications of combined CLI agents and radioactive/fluorescent agents in terms of preclinical studies are described in various papers [15–19].

As the introduction of optical imaging is relatively new in the field of nuclear medicine we address in this paper the general characteristics of luminescence (Fig. 1e) imaging and provide a physical quantitative evaluation of the two optical techniques. In addition, we relate the photophysical characteristics to relevant facets encountered during a clinical application in image-guided surgery.

Luminescence imaging and tissue penetration

We first introduce the limiting factors that luminescence imaging has compared to radionuclide imaging. Ideally, luminescence imaging yields a similar sensitivity as nuclear imaging technologies [20, 21]. However, other than the nuclear techniques, in the body luminescence signals suffer from a number of signal-reducing factors such as severe tissue attenuation. The severity of the attenuation depends on the wavelength of the emitted light; near-infrared (NIR) excitation and emission fit best to the optical transparency window of tissue (650–1,200 nm; Fig. 2e) [22]. Nevertheless, even in the

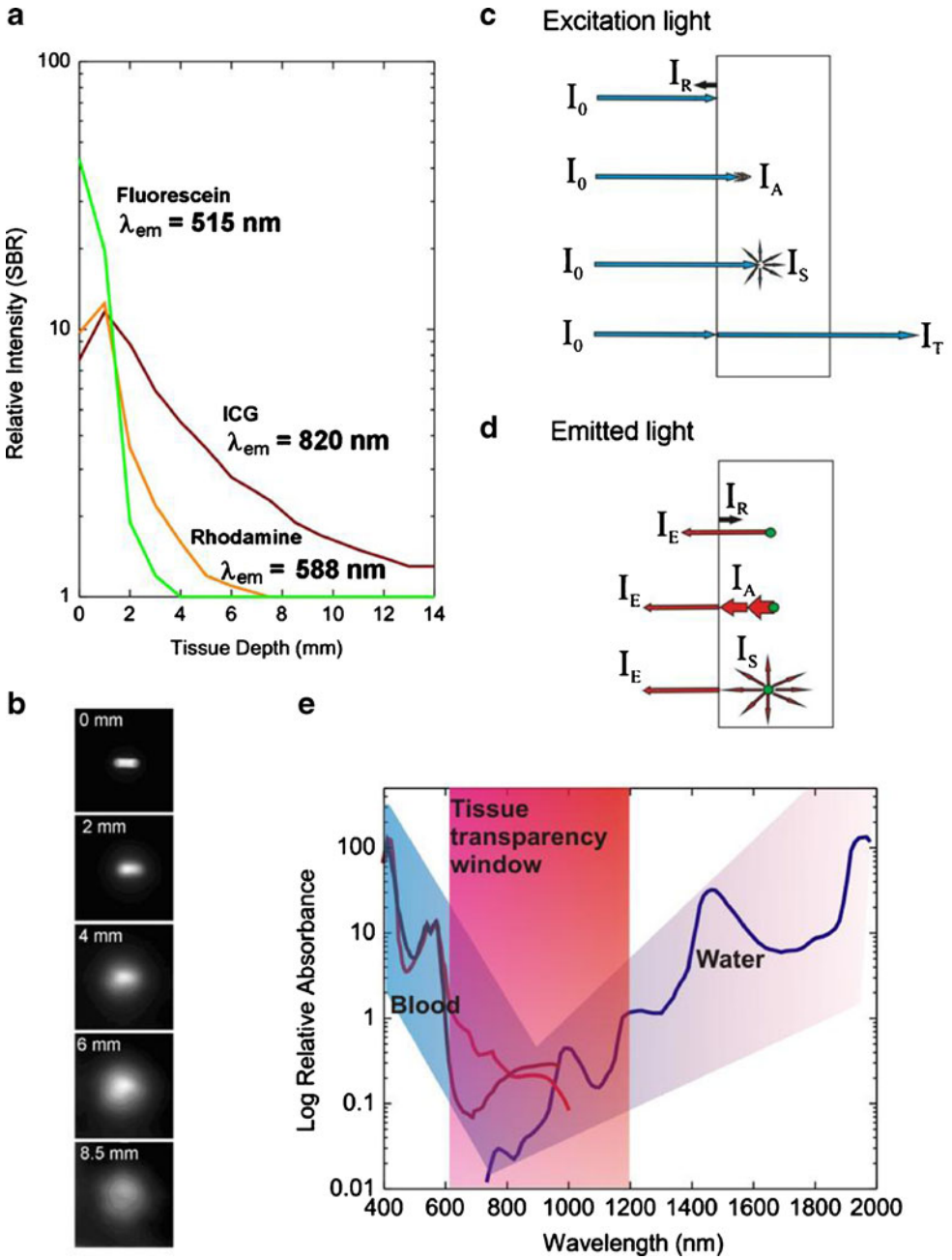

Fig. 2 **a** The relative fluorescence intensity (signal to background ratio, *SBR*) as a function of the tissue penetration of 0.5 mg/ml organic dye in a marker seed covered by increasing numbers of tenderloin [24]. **b** Example of the fluorescence signal scattering of an ICG-containing seed: the uncovered seed (0 mm) gives a signal comparable to the actual size of the seed, while covering the seed with layers of tenderloin tissue increases the diameter of the signal (1–8.5 mm) [24]. **c** Optical influences which can attenuate the excitation light (I_0), by absorbance (I_A), scattering (I_s) and surface reflection (I_r). **d** Furthermore, the emitted light is also attenuated by surface reflection (I_r), by absorbance (I_A) and scattering (I_s). **e** Tissue transparency optical window (650–1,200 nm) [22], largely determined by absorbance of (oxy)haemoglobin and water

transparency window the luminescence-based technologies are limited to superficial detection <1 cm [23, 24]. Tissue is very heterogeneous with respect to refractive index. Consequently, a significant portion of the emitted light will also suffer from scattering; shorter wavelengths will yield stronger scattering compared to the longer wavelengths [25]. Combined with surface reflections these factors result in a decrease in signal strength and imaging resolution with increasing tissue depth (Fig. 2a, b) [24].

When excitation light is required, autofluorescence (endogenous fluorescence of tissue) may generate a background signal that is not related to the imaging agent. This background signal may significantly reduce the signal to background ratios (SBRs) and thus the depth at which a luminescence signal has diagnostic value. UV/blue light <460 nm is the least favourable, as induced autofluorescence may yield significant background signals [26]. Other sources of background signals that are not related to the imaging agent are: ambient light, reflected/scattered excitation light and electronic noise that is generated by electrical dark currents in the camera [26, 27].

The absorbance of the luminescence by chromophores like haemoglobin strongly depends on the tissue type and location in the body. From Figs. 2e and 3 one can estimate that the UV/blue CL will suffer very severe signal attenuation in contrast to emissions within the tissue transparency window.

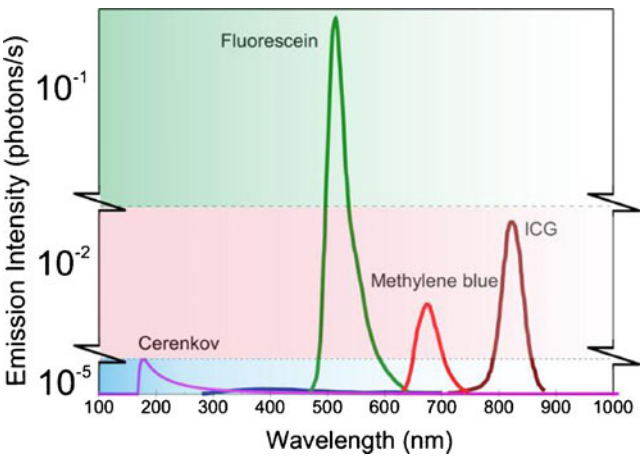

Fig. 3 Photophysical emissions of fluorescein, methylene blue and ICG compared to the CL from ^{18}F-FDG. Data from Table 1: fluorescein molecule (integrated photon flux of $\approx 10^{-1}$ photons/s) [41], methylene blue, ICG (integrated photon flux of $\approx 10^{-3}$ photons/s) and ^{18}F-FDG at clinically relevant conditions. The chromophores fluorescein (quantum yield=99 %), methylene blue (quantum yield=2 % in water) and ICG (quantum yield=2.7 % in water) excited using a 1 mW/cm^2 excitation source [47, 48]. The experimentally determined CLI signal (*blue line*) [29] and the theoretically predicted CLI signal (*pink line*). For simplicity the difference in tissue absorbance attenuation for the optical signals is neglected. The comparison between the CL and the fluorescence of fluorescein and ICG shows an intensity difference of 10^4 and 10^3, respectively

Quantitative comparison based on single molecule/isotope photon fluxes

Below we discuss the photophysical properties for both CL and fluorescence in image-guided surgery. To allow for a head-to-head comparison we perform the comparison based on the photon fluxes coming from a single isotope or molecule using photophysical calculations; we have included all the calculations in the "Electronic supplementary material" of the manuscript.

Cerenkov luminescence

CL [28] is originally known as the blue emission, which can be seen close to the nuclear fuel rods in nuclear power plants' cooling water basins. In contrast to fluorescence, the Cerenkov process is not based on the relaxation of a photoexcited molecular entity, meaning no optical activation is required. Rather, CL is induced by a charged β-particle travelling through a medium with a velocity greater than that of light in the same medium. Based on their energy charged β-particles can induce polarization of the molecules in the medium; upon relaxation of these molecules a photon is emitted (Fig. 1d). The emission curve of CL maximizes in the UV region of the spectrum (λ_{max} ~180 nm; water) (see Fig. 3); λ_{max} cannot be tuned towards other wavelengths.

Because CLI does not require external excitation, it does not suffer from autofluorescence or from the reflection of excitation light (Fig. 2b). Consequently, the amount of background signal is relatively low.

CL lies mostly within the UV and visible part of the spectrum [29]. Therefore CL cannot be separated by an integrating camera from the typically much brighter ambient light, which largely occurs in the same energy window. This means that (for sufficient SBR) CLI has to be performed in complete darkness; leakage of ambient (surgical) light will lead to a strong background signal and as a result a large reduction of the SBR. Preclinical CLI is performed using highly sensitive CCD cameras integrated in so-called black boxes [30, 31].

To determine the achievable CL intensity we first need to calculate the amount of Cerenkov photons produced by a single β-emitting isotope. Production of CL is a threshold effect that occurs only in the wavelength range and spatial location for which the square of the wavelength-dependent refractive index of the surrounding medium is larger than the inverse of the β-particle velocity divided by the speed of light, squared. The number of photons emitted then depends on the velocity and therefore the energy of the travelling β-particle and refractive index of the medium, as expressed by the Frank–Tamm formula (see "Electronic supplementary material", S.1.1. formula 1) [32, 33].

Although an increasing refractive index results in an increase in CL, this effect will be dominated by the location

of the lesion, which cannot be tuned. As the energy of the β-particle will influence the velocity, the amount of generated Cerenkov photons in vivo can only be improved by using high-energy β-emitters. For example, the most commonly applied ^{18}F PET tracer [positron end point energy; (β+) 633 keV] will produce 1.4 photons per decay (in water), while the therapeutic isotope ^{90}Y (β^- with an end point energy of 2.28 MeV) can produce up to 57 photons per decay in water [32].

Mitchell et al. [32] predicted a total photon flux of subsequently 9×10^6 and 250×10^6 photons/s^{-1} for a typical small animal experiment using either 3.6 MBq of ^{18}F or ^{90}Y. Assuming—for simplicity—that a single ^{18}F isotope decays within its half-life ($T_{1/2}$=109.7 min) it then corresponds to a photon flux of 2.1×10^{-4} photons/s^{-1} per isotope [34].

In this calculation the attenuation by absorbance and scattering is not taken into account; in practice the total flux of CL that can be detected will lie well below these predicted values as a result of tissue absorbance and scattering (Fig. 2e). Furthermore, similar to the nuclear imaging approaches, the CL intensity is also dependent on the half-life of the isotopes; hence, the signal intensity will go down in intensity over time (radioactive decay formula 2 in the "Electronic supplementary material", S1.1).

Due to the fact that the CL is a secondary emission, generated by a β-particle traveling through medium (Fig. 1d), the spatial resolution is lower than for fluorescence imaging. Monte Carlo simulations showed that the CL production is confined to a maximum of 2 mm for the isotopes with high end point energies (e.g. ^{90}Y) [13, 32]. Evidently tissue scattering may reduce this resolution even further.

Fluorescence

The use of the spontaneous emission of light radiation from a photoexcited molecular entity (fluorescence, Fig. 1e) in a systematic study of animal tissue was initially reported by Stübel in 1911 [35]. Since then the application of fluorescent molecules has become standard during preclinical molecular imaging applications (in vitro and in vivo) [36–38] and in medicine, where perfusion measurements using fluorescein [39] and indocyanine green (ICG) are routinely used [15, 40]. These fluorescent dyes (fluorophores) cover the most important spectral regions, e.g. fluorescein (green emission, λ_{max} ~515 nm) [41] and ICG (NIR emission, invisible to the human eye, λ_{max} ~820 nm).

The photophysical properties (excitation, emission, brightness) of fluorescent dyes depend on the molecular structure and can be fine-tuned by chemical modifications. The signal brightness of a fluorophore is proportional to the absorption coefficient (a quantity that characterizes the ease of penetration of light through a medium) multiplied by the quantum yield (the number of emitted photons per photon absorbed) [42]. For example, the visible dye fluorescein has an absorption coefficient of ≈8 10^4 l mol^{-1} cm^{-1} (at 490 nm) and a quantum yield close to unity, which corresponds to a brightness of ≈10^5. The NIR dye ICG, with an absorption coefficient of ≈1 10^5 l mol^{-1} cm^{-1} (at 780 nm, 6.5 μM) and a quantum yield of 2.7 %, only yields a brightness of ≈10^3.

The brightness gives an idea of the signal intensity of the light emitted by a fluorophore. However, the ability to detect this signal in an in vivo application depends on various physical parameters as shown in section S1.2 in the "Electronic supplementary material". A relatively high photon flux from the fluorophores with respect to the background signals will typically increase the detection sensitivity. As an illustration we have calculated the total expected photon flux from a single molecule of the commonly used clinical NIR dye ICG under a "realistic clinical" excitation power (1 mW/cm^2, "Electronic supplementary material", S1.2). These calculations show that under these conditions only a very small fraction of the molecules are in the excited state, namely 1.66×10^{-7} %. As a result per ICG molecule 4.6×10^{-2} photons/s^{-1} can be emitted. Both in preclinical and clinical applications, it has been shown that with sufficient ICG molecules at the area of interest a good signal intensity can still be obtained [6–8, 15, 38], sometimes even resulting in an SBR 1 >10 [24].

It should be noted that an increase of the excitation power will result in a linear increase of the fluorescence signal. For example, the FLARE [12] medical fluorescence system uses a 14 mW/cm^2 excitation source (including 50 % excitation attenuation by scattering) which will enhance the detectable luminescence intensity of a single ICG molecule with a factor of 7. Since these optical powers are relatively low compared to those used in microscopy, bleaching of the fluorophores and thus a loss in fluorescence intensity, in general, is not an issue.

Influence of scattering

The previously calculated photon fluxes of a single ^{18}F isotope and a single ICG molecule were not compensated for attenuation due to wavelength-dependent tissue scattering [25]. Even more so than with radioactive emissions, tissue scattering (Fig. 2) of luminescent signatures can significantly alter imaging sensitivity. Calculations based on only 1 mm of tissue depth resulted in a 77 and 39 % reduction in the signal intensity for one ^{18}F-isotope and one ICG molecule, respectively (see Table 1; for the calculations see the "Electronic supplementary material", S2).

Camera sensitivity

The detection sensitivity of the camera systems plays a crucial role in the (medical) implementation of the luminescence imaging technology. CCD-based imaging sensors can

Table 1 A quantitative comparison between the single molecule photon fluxes of commonly applied CLI isotopes and three clinically available fluorophores

Material	Initial intensity (for fluorescence under 1 mW/cm^2 excitation intensity) (photons s^{-1} n^{-1})	Intensity through 1 mm of scattering tissue (photons s^{-1} n^{-1})	Corrected for typical camera sensitivity range (CCD) [43] sensitivity (photons s^{-1} n^{-1})
^{90}Y	2.5×10^{-4}	5.5×10^{-5}	2.8×10^{-5}
^{18}F	2.1×10^{-4}	4.8×10^{-5}	2.4×10^{-5}
Fluorescein	7.4×10^{-1}	2.7×10^{-1}	2.3×10^{-1}
ICG	4.6×10^{-2}	2.8×10^{-2}	2.2×10^{-2}
Methylene blue	2.4×10^{-2}	1.2×10^{-2}	1.1×10^{-2}

n single molecule or single isotope

have quantum efficiencies above 92 % in the optimal spectral region ~570–720 nm. This spectral region is sufficient for the most common luminescent molecules. Unfortunately, the efficiency of these systems is nearly reduced to half in the range where the CL is most intense (λ<350 nm). Although the influence is less dramatic for NIR dyes, above 800 nm the efficiency is typically reduced to 80 % [43]. This effect will further reduce the signal intensities (see Table 1 and Fig. 3).

Clinical value of hybrid imaging technologies

Using common sentinel node biopsy procedures, we have demonstrated the clinical value that hybrid imaging agents can provide. Other than solely luminescent compounds, a hybrid compound that has both radioactive and luminescent signatures allows use in radionuclear diagnostics, e.g. lymphoscintigraphy, SPECT/CT, gamma probe tracing, freehand SPECT and/or a portable gamma camera (Figs. 1 and 4) [8]. In combination with the right camera system, during surgery, the luminescent component of the tracer then enables optical identification of the areas of interest and their margins. This has proven efficient in both an open and laparoscopic setting [7, 8]. We found that the real-time information [24–48 frames per second (fps)] and the high spatial resolution, provided by the luminescent signature, were particularly valuable [7, 8].

Our experience is that the added value of fully integrated optical guidance is most prominent in indications where the patient's anatomy is complex [8, 44, 45] and /or when the surgeon's senses are reduced, e.g. laparoscopy [45]. Uniquely, in a hybrid compound the shortcomings of the individual modalities are compensated. For example, the radioactive signal penetration, which makes it of value for preoperative and in-depth diagnostics, in some indications limits the surgical identification. Here the limited tissue penetration of luminescent signatures allows the identification of nodes that are located close to the injection site [7, 8, 44, 45].

It is important to note that for such hybrid procedures there is no increase in the amount of radioactivity compared to what is commonly used with the parent radiotracer [45]. Moreover, we have already shown that decay of the radioactive signature does not limit the fluorescence-based detection [46].

Clinical availability of hybrid imaging agents

Due to the recent clinical availability of light-sensitive surgical cameras, optical surgical guidance is attracting a lot of

Fig. 4 Sentinel lymph node identification using synchronous radioactive/fluorescence signal detection in a patient with a carcinoma in the apical area of the tongue. **a** Volume rendering SPECT/CT showing lymphatic drainage to the right side of the neck. **b** After skin incision the sentinel node is localized in the operative field using an NIR fluorescence camera, followed by real-time visualization on a video screen (**c**)

attention. Availability of dedicated imaging agents, however, is still limited. Fluorescein, methylene blue and ICG are the clinically approved fluorophores that are most widely available [47, 48]. Unfortunately, these fluorophores cannot be covalently attached to a (targeting) molecular scaffold, thus limiting their use in hybrid imaging agents to non-covalent assemblies like ICG-^{99m}Tc-nanocolloid [6, 7]. To generate e.g. tumour-targeted hybrid imaging agents, new synthetic strategies, using a variety of fluorophores and chelates/isotopes, have been designed [49]. Unfortunately, to date these new compounds have not yet become available for clinical use.

The large variation of already clinically approved β-particle emitters may help to significantly expand the field of hybrid imaging agents without requiring the clinical translation of new chemical entities [50]. In this sense CLI has the potential to significantly enlarge the clinical implementation of hybrid imaging approaches; Grimm and Schöder recently registered a clinical trial, using ^{18}F-fluorodeoxyglucose (^{18}F-FDG) and ^{131}I for Cerenkov-based head and neck tumour visualization [51].

Limitations of CLI

To enable a clear comparison between the different types of hybrid imaging agents we have summarized their radioactive and luminescent properties in Table 2. Below we discuss the—in our opinion—biggest limitations of CLI compared to the use of hybrid imaging agents based on common (NIR) fluorophores.

Due to the limited tissue penetration of light with a wavelength below 450 nm, for in vivo applications CLI will most likely be limited to a very superficial tissue depth, meaning that the area of interest has to be fully exposed prior to imaging. In the preclinical setting acquisition times between 1 and 5 min were reported to obtain CLI images with a sufficient SBR [18, 19]. Hence, with the current

Table 2 Typical nuclear and optical properties of hybrid and Cerenkov probes

	Hybrid	Cerenkov
Multimodal properties		
Combined pre- and intraoperative imaging	Yes	(Potentially) yes
Preoperative imaging systems	Gamma camera, SPECT or PET	Gamma camera, SPECT or PET
Intraoperative modalities	γ (annihilation) photons, β^+ positrons, fluorescence	γ (annihilation) photons, β^+ positrons, CL
Nuclear properties		
Commonly clinically applied imaging isotopes	SPECT & PET ^{99m}Tc, ^{68}Ga, ^{123}I, ^{111}In, ^{18}F, ^{64}Cu, ^{89}Zr, ^{124}I	PET & β emitters ^{18}F, ^{64}Cu, ^{89}Zr, ^{124}I, ^{90}Y, ^{131}I
Label size	Molecular	Single atom
Decay pathway	γ, β^+	β^+, β^-
Typical energy range	γ≈100–511 keV	γ: 511 keV γ: 364 keV β: 0.250–2.28 MeV
Typical clinical dose	Adults: 100–600 MBq Children: 10–200 MBq	≈9.7 GBq ^{18}F-FDG predicted for 70 kg adults [52], corrected for a 4-h time delay between injection and surgery
Penetration depth nuclear signal	10 cm–m	10 cm–m
Optical properties		
Estimated signal strength single molecule/isotope without tissue absorbance	0.2–0.01 (at 1 mW/cm^2 excitation intensity)	0.00002–0.00003
Luminescence penetration depth	<10 mm	Not known (probably <1 mm)
Resolution	0.2 μm[a]	0.2 μm–2 mm
Excitation source	LED/laser/incandescent lamps and xenon lamps	n.a.
Typical optical excitation range	400–800 nm	n.a.
Emission detection	Standard (laparoscopic) camera or naked eye	Ultra-high sensitivity camera (not yet clinically available)
Emission maxima	λ_{max} 520–820 nm (tunable)	λ_{max} 180 nm
Typical image acquisition time	<42 ms (real time)	>min

[a] Defined by optical diffraction limit of light. Optical techniques like stimulated emission depletion (STED) can enhance the optical resolution further to <20 nm

technology real-time optical detection is very unlikely. Also, creating complete darkness, while preserving a sterile environment, is not easy. An endoscopic setting would enable a darker environment; unfortunately, the acceptance cone of the endoscopic system generally also results in another 40–50 % loss of the detectible photon flux [53].

Liu et al. predicted the necessity of high tracer doses for CLI [54]. They calculated that a 70 kg patient would require a surgical dose of 2.1 GBq of ^{18}F-FDG. Unfortunately, the half-life of the isotope decreases the signal intensity over time (see Eq. 2). Since the first CLI session in the operating room occurs realistically 4 h post-injection, the patient would acquire an incredibly high dose. The example proposed by Liu et al. [54] will then require ≈9.7 GBq ^{18}F-FDG. Alternatively one may use higher energy isotopes. Both, however, increase the radiation burden for the patient, the surgical team and the pathology staff.

Technical improvements for CLI

(Bio-) fluorescence imaging was already reported in 1911 [35], whereas surgical fluorescence imaging just recently became widely available. CLI was only recently introduced (2009) [19, 32]. As CLI still is a very immature technology, similar improvements in the technology are likely to occur.

One improvement may be selective light conversion using luminescent nanoparticles that convert the CL to a single narrow emission band, positioned within the tissue transparency window [52]. Such light conversion technologies enable the use of bandpass filters for detection, reducing the influence of ambient light. When combined with ongoing developments of imaging sensors for ultra-low light detection (e.g. EMCCD) and the use of endoscopic techniques [53, 54] this approach may improve the detection sensitivity.

Conclusion

Hybrid imaging agents based on the combination of a radioisotope and a fluorophore have already proven their value in image-guided surgery applications. Cerenkov-based hybrid imaging agents unfortunately have much lower luminescence intensities, making their success depend on the new technical developments that are currently being made in this exciting research line.

Acknowledgments This work was financially supported by the division of Chemical Sciences (CW) of the Dutch Science Foundation (NWO) under grant number VENI 722.011.005 (PC) and NWO-STW-VIDI (Grant No. STW BGT11271; FvL).

Conflicts of interest None.

References

1. Phelps ME. PET: the merging of biology and imaging into molecular imaging. J Nucl Med 2000;41:661–81.
2. Histed SN, Lindenberg ML, Mena E, Turkbey B, Choyke PL, Kurdziel KA. Review of functional/anatomical imaging in oncology. Nucl Med Commun 2012;33:349–61.
3. Kim WW, Kim JS, Hur SM, Kim SH, Lee S-K, Choi JH, et al. Radioguided surgery using an intraoperative PET probe for tumor localization and verification of complete resection in differentiated thyroid cancer: a pilot study. Surgery 2011;149:416–24.
4. Wahl RL, Quint LE, Cieslak RD, Aisen AM, Koeppe RA, Meyer CR. "Anatometabolic" tumor imaging: fusion of FDG PET with CT or MRI to localize foci of increased activity. J Nucl Med 1993;34:1190–7.
5. Ichise M, Chung D-G, Wang P, Wortzman G, Gray BG, Franks W. Technetium-99m-HMPAO SPECT, CT and MRI in the evaluation of patients with chronic traumatic brain injury: a correlation with neuropsychological performance. J Nucl Med 1994;35:217–26.
6. Buckle T, van Leeuwen AC, Chin PTK, Janssen H, Muller SH, Jonkers J, et al. A self-assembled multimodal complex for combined pre- and intraoperative imaging of the sentinel lymph node. Nanotechnology 2010;21:355101.
7. van der Poel HG, Buckle T, Brouwer OR, Valdés Olmos RA, van Leeuwen FWB. Intraoperative laparoscopic fluorescence guidance to the sentinel lymph node in prostate cancer patients: clinical proof of concept of an integrated functional imaging approach using a multimodal tracer. Eur Urol 2011;60:826–33.
8. van den Berg NS, Brouwer OR, Klop WMC, Balm AJ, van den Brekel M, Valdés Olmos RA, et al. A hybrid tracer for concomitant radio- and fluorescence guided sentinel lymph node biopsy in oral cavity cancer. J Nucl Med 2012;53(Suppl 1):1666.
9. Chang H-C, Chung C-K. The development of fluorescence imaging systems for clinical applications—part I, broad-field fluorescence imaging. Int J Instrum Sci 2012;1:16–20.
10. van den Berg NS, van Leeuwen FWB, van der Poel HG. Fluorescence guidance in urologic surgery. Curr Opin Urol 2012;22:109–20.
11. Magnan P. Detection of visible photons in CCD and CMOS: a comparative view. Nucl Instrum Methods Phys Res A 2003;504:199–212.
12. Troyan SL, Kianzad V, Gibbs-Strauss SL, Gioux S, Matsui A, Oketokoun R, et al. The FLARE™ intraoperative near-infrared fluorescence imaging system: a first-in-human clinical trial in breast cancer sentinel lymph node mapping. Ann Surg Oncol 2009;16:2943–52.
13. Spinelli AE, Boschi F. Optimizing in vivo small animal Cerenkov luminescence imaging. J Biomed Opt 2012;17:040506.
14. Robertson R, Germanos MS, Li C, Mitchell GS, Cherry ST, Silva MD. Optical imaging of Cerenkov light generation from positron-emitting radiotracers. Phys Med Biol 2009;54:N355–65.
15. van Leeuwen AC, Buckle T, Bendle G, Vermeeren L, Valdés Olmos R, van der Poel HG, et al. Tracer-cocktail injections for combined pre- and intraoperative multimodal imaging of lymph nodes in a spontaneous mouse prostate tumor model. J Biomed Opt 2011;16:016004.
16. Bhushan KR, Misra P, Liu F, Mathur S, Lenkinski RE, Frangioni JV. Detection of breast cancer microcalcifications using a dual-modality SPECT/NIR fluorescent probe. J Am Chem Soc 2008;130:17648–9.
17. Thorp-Greenwood FL, Coogan MP. Multimodal radio- (PET/SPECT) and fluorescence imaging agents based on metallo-radioisotopes: current applications and prospects for development of new agents. Dalton Trans 2011;40:6129–43.

18. Xu Y, Chang E, Liu H, Jiang H, Gambhir SS, Cheng Z. Proof-of-concept study of monitoring cancer drug therapy with Cerenkov luminescence imaging. J Nucl Med 2012;53:312–7.
19. Holland JP, Normand G, Ruggiero A, Lewis JS, Grimm J. Intraoperative imaging of positron emission tomographic radiotracers using Cerenkov luminescence emissions. Mol Imaging 2011;10:177–86.
20. Culver J, Akers W, Achilefu S. Multimodality molecular imaging with combined optical and SPECT/PET modalities. J Nucl Med 2008;49:169–72.
21. Alford R, Ogawa M, Choyke PL, Kobayashi H. Molecular probes for the in vivo imaging of cancer. Mol Biosyst 2009;5:1279–91.
22. Huang Y-Y, Chen AC-H, Hamblin M. Low-level laser therapy: an emerging clinical paradigm. SPIE Newsroom. doi:10.1117/2.1200906.1669.
23. Lubart R, Lavie R, Friedman H. The penetration of white light through human tissue. Photomed Laser Surg 2005;23:435–6.
24. Chin PTK, Beekman CA, Buckle T, Josephson L, van Leeuwen FWB. Multispectral visualization of surgical safety-margins using fluorescent marker seeds. Am J Nucl Med Mol Imaging 2012;2:151–62.
25. Mourant JR, Fuselier T, Boyer J, Johnson TM, Bigio IJ. Predictions and measurements of scattering and absorption over broad wavelength ranges in tissue phantoms. Appl Opt 1997;36:949–57.
26. Andersson-Engels S, Klinteberg C, Svanberg K, Svanberg S. In vivo fluorescence imaging for tissue diagnostics. Phys Med Biol 1997;42:815–24.
27. Reibel Y, Jung M, Bouhifd M, Cunin B, Draman C. CCD or CMOS camera noise characterisation. Eur Phys J Appl Phys 2003;21:75–80.
28. Cerenkov PA. Visible radiation produced by electrons moving in a medium with velocities exceeding that of light. Phys Rev 1937;52:378–9.
29. Cho JS, Taschereau R, Olma S, Liu K, Chen YC, Shen CKF, et al. Cerenkov radiation imaging as a method for quantitative measurements of beta particles in a microfluidic chip. Phys Med Biol 2009;54:6757–71.
30. Wu JC, Sundaresan G, Iyer M, Gambhir SS. Noninvasive optical imaging of firefly luciferase reporter gene expression in skeletal muscles of living mice. Mol Ther 2001;4:297–306.
31. Contag CH, Spilman SD, Contag PR, Oshiro M, Eames B, Dennery P, et al. Visualizing gene expression in living mammals using a bioluminescent reporter. Photochem Photobiol 1997;66:523–31.
32. Mitchell GS, Gill RK, Boucher DL, Li C, Cherry SR. In vivo Cerenkov luminescence imaging: a new tool for molecular imaging. Philos Transact A Math Phys Eng Sci 2011;369:4605–19.
33. Frank IM, Tamm IE. Coherent visible radiation of fast electrons passing through matter. Dokl Akad Nauk SSSR 1937;14:109–14.
34. Pfennig G, Klewe-Nebenius H, Seelmann-Eggebert W. Karlsruher Nuklidkarte. 6th ed. Lage: Haberbeck; 1998.
35. Stübel H. Die Fluoreszenz tierischer Gewebe in ultravioletten Licht. Pflugers Arch Physiol 1911;142:1–14.
36. Weissleder R, Ntziachristos V. Shedding light onto live molecular targets. Nat Med 2003;9:123–8.
37. Ntziachristos V. Fluorescence molecular imaging. Annu Rev Biomed Eng 2006;8:1–33.
38. Frangioni JV. In vivo near-infrared fluorescence imaging. Curr Opin Chem Biol 2003;7:626–34.
39. Moore GE, Peyton WT, French LA, Walker WW. The clinical use of fluorescein in neurosurgery; the localization of brain tumors. J Neurosurg 1948;5:392–8.
40. Alander JT, Kaartinen I, Laakso A, Pätilä T, Spillmann T, Tuchin VV, et al. A review of indocyanine green fluorescent imaging in surgery. Int J Biomed Imaging 2012;2012:940585.
41. Martin MM, Lindqvist L. The pH dependence of fluorescein fluorescence. J Lumin 1975;10:381–90.
42. Lavis LD, Raines RT. Bright ideas for chemical biology. ACS Chem Biol 2008;3:142–55.
43. Concepts in digital imaging technology quantum efficiency http://learn.hamamatsu.com/articles/quantumefficiency.html.
44. Brouwer OR, Klop MWC, Buckle T, Vermeeren L, van den Brekel MWM, Balm FJM, Nieweg OE, et al. Feasibility of sentinel node biopsy in head and neck melanoma using a hybrid radioactive and fluorescent tracer. Ann Surg Oncol 2012;19:1988–94.
45. Brouwer OR, Buckle T, Vermeeren L, Klop WMC, Balm AJM, van der Poel HG, et al. Comparing the hybrid fluorescent-radioactive tracer indocyanine green-99mTc-nanocolloid with 99mTc-nanocolloid for sentinel node identification: a validation study using lymphoscintigraphy and SPECT/CT. J Nucl Med 2012;53:1034–40.
46. Buckle T, Brouwer OR, Valdés Olmos RA, van der Poel HG, van Leeuwen FWB. Relation between intraprostatic tracer deposits and sentinel lymph node mapping in prostate cancer patients. J Nucl Med 2012;53:1026–33.
47. Lee S-K, Mills A. Luminescence of leuco-thiazine dyes. J Fluoresc 2003;13:375–7.
48. Landsman MLJ, Kwant G, Mook GA, Zijlstra WG. Light-absorbing properties, stability, and spectral stabilization of indocyanine green. J Appl Physiol 1976;40:575–83.
49. Kuil J, Velders AH, van Leeuwen FWB. Multimodal tumor-targeting peptides functionalized with both a radio- and a fluorescent-label. Bioconjug Chem 2010;21:1709–19.
50. Ruggiero A, Holland JP, Lewis JS, Grimm J. Cerenkov luminescence imaging of medical isotopes. J Nucl Med 2010;51:1123–30.
51. Grimm J, Schöder H. Non-invasive Cerenkov luminescence imaging of lymphoma, leukemia and metastatic lymph nodes. 2012. http://www.ClinicalTrails.gov, Identifier: NCT01664936.
52. Dothager RS, Goiffon RJ, Jackson E, Harpstrite S, Piwnica-Worms D. Cerenkov radiation energy transfer (CRET) imaging: a novel method for optical imaging of PET isotopes in biological systems. PLoS One 2010;5:e13300.
53. Kothapalli S-R, Liu H, Liao JC, Cheng Z, Gambhir SS. Endoscopic imaging of Cerenkov luminescence. Biomed Opt Express 2012;3:1215–25.
54. Liu H, Carpenter CM, Jiang H, Pratx G, Sun C, Buchin MP, et al. Intraoperative imaging of tumors using Cerenkov luminescence endoscopy: a feasibility experimental study. J Nucl Med 2012;53:1579–84.